Available online at www.sciencedirect.com
ScienceDirect
Trans. Nonferrous Met. Soc. China 35(2025) 2874−2885
Transactions of Nonferrous Metals Society of China
www.tnmsc.cn

Effect of high pressure on microstructure and microsegregation of Mg−11Al alloys

Shi-min AI[1], Xiao-ping LIN[1,2], Yao-wei GUO[1], Xu-zhao ZHANG[1], Da-ran FANG[1,2], Lian-wei YANG[1,2], Bin WEN[3]

1. School of Materials Science and Engineering, Northeastern University, Shenyang 110819, China;
2. School of Resources and Materials, Northeastern University at Qinhuangdao, Qinhuangdao 066004, China;
3. School of Materials Science and Engineering, Yanshan University, Qinhuangdao 066004, China

Received 7 January 2024; accepted 2 August 2024

Abstract: The effect of high pressure on the microstructure and microsegregation of Mg−11Al (mass fraction, %) alloys was studied through experiments and first-principles calculations. The results show that the Al content in the initial solid phase is high owing to the high solute partition coefficient and the large undercooling in the alloys solidified under pressures of 4−6 GPa, and the Al content in the initial solid phase increases with the increase of pressure. Consequently, the total amount of excess solute in the liquid phase in the final solidification stage decreases with increasing pressure, thus decreasing or suppressing the eutectic transformation. Furthermore, the microstructure of the alloys solidified under pressures of 5−6 GPa is a fine-grained solid solution, consisting of grains with high solubility of Al atoms and grain boundaries with abundant Al solutes. As the pressure increases, the grain boundary doping energy of Al atoms decreases, while their grain boundary segregation energy of Al atoms increases, and the charge density between the Mg—Al (Mg) bonds also rises. Therefore, the stability of the microstructure is improved, and the bond strength of grain boundaries is enhanced.

Key words: high-pressure solidification; grain boundary segregation; partition coefficient; Mg−Al alloy; solid solution

1 Introduction

The cast Mg−Al alloys have been widely used in industry and are important in the research field of magnesium alloys [1,2]. For AZ91D alloy, a typical Mg−Al alloy, a large amount of reticulate eutectic phase β-$Mg_{17}Al_{12}$ occurs at α-Mg grain boundaries due to grain boundary segregation of Al atoms during solidification, resulting in poor ductility and low ultimate strength of the alloy [3]. Therefore, the mechanical properties of Mg−Al alloys are closely related to the morphology, distribution, and quantity of β-$Mg_{17}Al_{12}$ phase. According to previous research, adding trace elements such as Ca [4], Sr [5], and RE [6] is a feasible method to improve the morphology, distribution, and size of the eutectic phase. However, the improvements in the mechanical properties of the alloy are limited. Thus, it is necessary to develop high-performance cast Mg−Al alloys to decrease the grain boundary segregation of Al atoms and inhibit the formation of β-$Mg_{17}Al_{12}$.

Microsegregation arises from the solute redistribution during alloy solidification, and the degree of microsegregation primarily depends on the solute equilibrium partition coefficient (k_0). For alloys with k_0<1, the severity of the microsegregation increases with decreasing k_0 [7]. Thus, increasing k_0 of the alloys is an effective method to reduce microsegregation when the chemical composition remains unchanged. According to the

Corresponding author: Xiao-ping LIN, Tel: +86-13780356091, E-mail: lxping3588@163.com
https://doi.org/10.1016/S1003-6326(25)66854-3

metal solidification theory, the solute equilibrium distribution coefficient k_0 is the ratio of the solute concentration in the solid phase (C_S) to the solute concentration in the liquid phase (C_L) in an equilibrium state at a constant temperature [8]. Therefore, k_0 will be affected by pressure, which is similar to the melting point of metals. SOBCZAK et al [9] studied the effect of high pressure on the phase diagram of Al−Si binary alloys and found that the maximum solid solubility of Si atoms in the Al matrix and Si content at the eutectic point increased with increasing solidification pressure. Moreover, the maximum solid solubility increased at a higher rate than the Si content at the eutectic point. JIE et al [10] investigated the microstructure of the Al−32at.%Mg eutectic alloy solidified under 3 GPa pressure, and the results showed that the microstructure consisted of a supersaturated α-Al solid solution and a little island-like eutectic phase distributed among dendrites. LIN et al [11] reported the effect of high pressure on the solidification structure of Mg−Zn−Y alloys and found that the eutectic phase in the alloy solidified under atmospheric pressure appeared reticulate, while the eutectic phase in the alloy solidified under 3 GPa pressure exhibited a morphology of discontinuous islands. XU et al [12] studied the effect of the β-$Mg_{17}Al_{12}$ eutectic phase on the mechanical properties of Mg alloys solidified under different pressures and demonstrated that the Al content required for the eutectic transformation among α-Mg dendrites increased from 7 wt.% at atmospheric pressure to 15 wt.% at 4 GPa. They also found that high pressure significantly reduced eutectic phase spacing. Accordingly, high-pressure solidification can effectively reduce the grain boundary segregation and improve the microstructure of alloys [13], which offers a promising method of suppressing the formation of the eutectic phase β-$Mg_{17}Al_{12}$.

The maximum solid solubility of Al atoms is 11.2 wt.% according to the Mg−Al binary equilibrium phase diagram, so Mg−11Al alloy (mass fraction, %) was prepared in this study. The microstructure, grain size, Al solute distribution, and grain boundary segregation in the Mg−11Al alloy solidified under high pressure (2−6 GPa) were investigated, and the effect of the pressure on solute redistribution during solidification of the Mg−11Al alloy was discussed. By means of experimental research and first-principles calculations based on density functional theory (DFT), the effect of the pressure on grain boundary doping energy and grain boundary segregation energy of Al atoms was expounded, and the relationship between grain boundary segregation of Al solute and the bonding strength of grain boundaries was analyzed. We conducted in-depth research on the high-pressure solidification of Mg alloys and developed a new type of Mg−Al alloy based on grain boundary segregation of Al solute, which is extremely significant for the design idea and toughening theory of Mg alloys.

2 Experimental

The Mg−Al ingots were prepared from pure Mg (purity 99.95%) and pure Al (purity 99.95%) using vacuum smelting equipment. The melting temperature was set to be 680 °C, according to the liquidus temperature of the Mg−Al binary alloy. After the metals were completely melted and held for 20 min, the molten liquid was poured into a graphite mold, producing ingots with a diameter of 22 mm and a length of 150 mm. The Al content of the ingots was 10.88 wt.%, as measured by ICAP6300 plasma spectrometry. Afterward, rods with a diameter of 6 mm and a length of 10 mm were cut from the ingots by spark cutting.

High-pressure solidification experiments were performed using a CS−1V hexahedral hydraulic ram, as shown in Fig. 1.

The rod was placed in the graphite sleeve, which was then inserted into the cavity of the hexahedral hydraulic ram. The hammers were placed facing the sample. The pressure was increased to the preset value while the rod was rapidly heated to the preset temperature. After maintaining the temperature and pressure for 20 min, the power supply was turned off. The cooling rate was controlled by adjusting the flow rate of the cooling water. Finally, the alloy was cooled to room temperature while maintaining pressure. The solidification pressure was set between 2 and 6 GPa. The heating temperatures were determined according to the Clausius–Clapeyron equation [14] and the change in melting point under pressure (Mg, 63.8 K/GPa) [15]. The temperatures were as follows: (720±10) °C at 2 GPa, (780±10) °C at 3 GPa, (850±10) °C at 4 GPa,

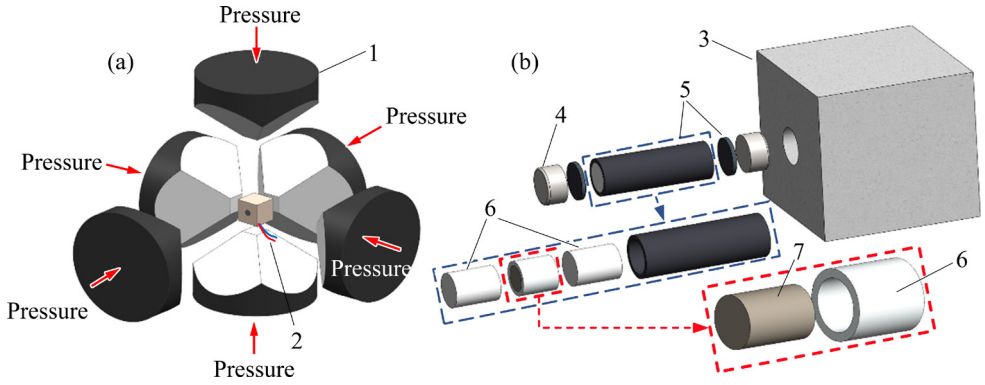

Fig. 1 Schematic diagrams of working principle of CS-1V type six-anvil apparatus (a) and high-pressure solidification assembly (b): 1—Anvil; 2—Thermocouple wire; 3—Pyrophyllite; 4—Conductive cap; 5—Graphite; 6—Boron nitride; 7—Rod

(910±10) °C at 5 GPa, and (980±10) °C at 6 GPa. The Clausius–Clapeyron equation is as follows [14]:

$$dP/dT_m=\Delta H/T_m\Delta V \quad (1)$$

where P is the pressure, T_m is the melting temperature, $\Delta V=V_l-V_S$ is the difference between liquid and solid in specific volumes, and ΔH is the specific heat of fusion.

The microstructure was observed using scanning electron microscopy (SEM, ZEISS SAPPHIRE SUPRA 55). The chemical composition was analyzed using an energy-dispersive X-ray spectroscope (EDS, Oxford X-MaxN 50) attached to the SEM. The area fraction of the secondary phase was calculated using Image-Pro-Plus software. The phase analysis was performed using X-ray diffractometer (XRD, Rigaku Smart Lab); the angle range was 20°−90°, and the scan rate was 2 (°)/min.

The atomic configuration of the alloy was optimized using the Vienna ab initio simulation package (VASP) [16] based on density functional theory (DFT) to obtain an atomic configuration with the lowest energy. In addition, the interaction between ions and electrons was described by the projector augmented wave method, and the exchange-correlation function was discussed with the help of the generalized gradient approximation (GGA) [17]. According to the Monkhorst–Pack method, automatic sampling in the Brillouin zone was centered on a 4×8×1 Γ point. The cut-off energy was 600 eV, the energy convergence criterion was that the energy difference between adjacent electronic steps was less than 1.0×10^{-5} eV, and the force convergence criterion was that the force exerted on every atom in the system was less than 1.0×10^{-2} eV/Å. The supercell (11 Å × 7 Å × 37 Å) composed of 120 Mg atoms was constructed using Materials Studio software, and the atomic configuration of the symmetric tilt grain boundary is shown in Fig. 2. The blue spheres in Fig. 2 represent Al atoms doped at compression sites.

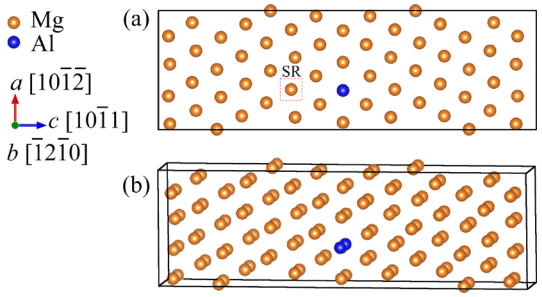

Fig. 2 Atom configurations of symmetric tilt grain boundary: (a) 2D model; (b) 3D model

3 Results and discussion

3.1 Effect of solidification pressure on micro-segregation of Mg−11Al alloy

Figures 3(a, b) show the microstructure of the Mg−11Al alloy solidified under atmospheric pressure, and Fig. 3(c) shows an EDS map of the element Al in the area of Fig. 3(b). Figure 4 shows the XRD patterns of the alloys solidified at different pressures. From Figs. 3 and 4, it can be seen that the microstructure is composed of equiaxed α-Mg grains, eutectic structure (α-Mg + β-$Mg_{17}Al_{12}$ shown in the inset in Fig. 3(a)), and lamellar β-$Mg_{17}Al_{12}$ phase (the inset in Fig. 3(b)). The average grain size of α-Mg is approximately 126 μm. The eutectic β-$Mg_{17}Al_{12}$ and the lamellar β-$Mg_{17}Al_{12}$ are

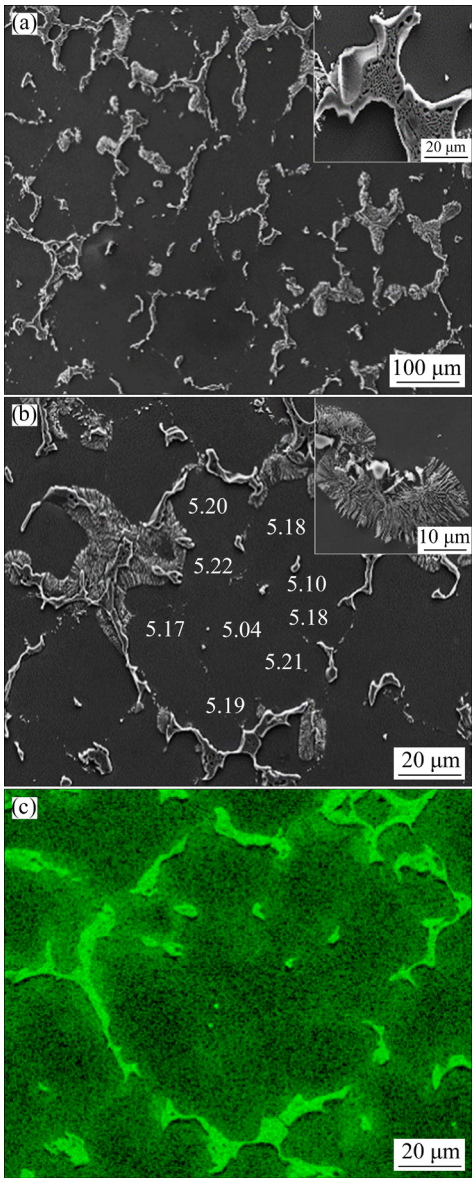

Fig. 3 Microstructure of Mg−11Al alloy solidified under atmospheric pressure (a, b), and EDS map of element Al (c)

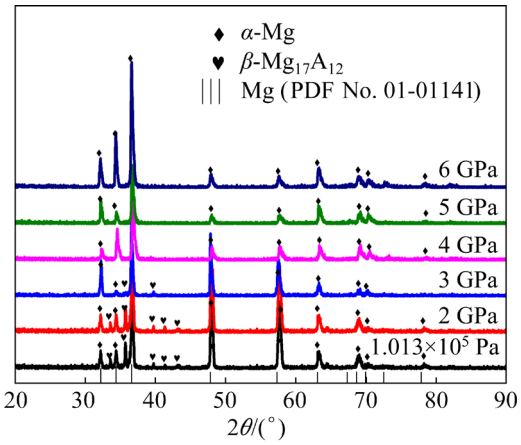

Fig. 4 XRD patterns of alloys solidified under different pressures

distributed along the grain boundaries of α-Mg grains owing to severe grain boundary segregation of Al atoms (shown in Fig. 3(c)), appearing reticulate. Moreover, it can be calculated that the area fraction of the β-$Mg_{17}Al_{12}$ phase is approximately 21%. According to the EDS data (the numbers in Fig. 3(b) indicate the Al content at each location), the average Al content at the center of the grains and near the grain boundaries is 5.04 wt.% and 5.19 wt.%, respectively. Thus, the average Al content at the center of the grains was greater than 4.07 wt.% of k_0C_0 (C_0 is the alloy composition in wt.%), and the dendritic segregation ratio (S_R) was 1.02.

Figure 5 shows the microstructure and EDS maps of the Mg–11Al alloy solidified under pressures of 2 and 3 GPa. According to Fig. 5(a) and Fig. 4, the microstructure of the alloy solidified under 2 GPa is composed of α-Mg and β-$Mg_{17}Al_{12}$, and the average grain size of α-Mg decreases to 85 μm compared with the alloy solidified under atmospheric pressure. As shown in Figs. 5(a, b), the area fraction of island-like eutectic β-$Mg_{17}Al_{12}$ at the grain boundaries is reduced (13.2%), and there is no lamellar β-$Mg_{17}Al_{12}$ phase near the grain boundaries. Moreover, plenty of island-like or granular eutectic β-$Mg_{17}Al_{12}$ can be observed among dendrites because of severe dendritic segregation (Fig. 5(c)). According to the EDS data (the numbers in Fig. 5(b) indicate the Al content at each location), the average Al content at the center of the grains and near the grain boundaries is 5.24 wt.% and 6.73 wt.%, respectively.

When the pressure is increased to 3 GPa, the microstructure of the alloy is further refined, and the average grain size decreases to 70 μm, as shown in Fig. 5(d). The grain shape of α-Mg is more regular, and the granular eutectic β-$Mg_{17}Al_{12}$ is distributed at the grain boundaries. The area fraction of eutectic β-$Mg_{17}Al_{12}$ further decreases (8.1%). As shown in Fig. 5(e), the Al content at the center of the grains is 5.35 wt.%, while the Al content near the grain boundaries (the area without eutectic phase) changes from 10.5 wt.% to 13.87 wt.%. The dendrite segregation ratio is 2.17, which is higher than that of the alloy solidified under atmospheric pressure (1.02).

For the alloys solidified under 4, 5, and 6 GPa, the average grain size continually decreases to 61, 50, and 46 μm, respectively, as shown in Fig. 6. Under

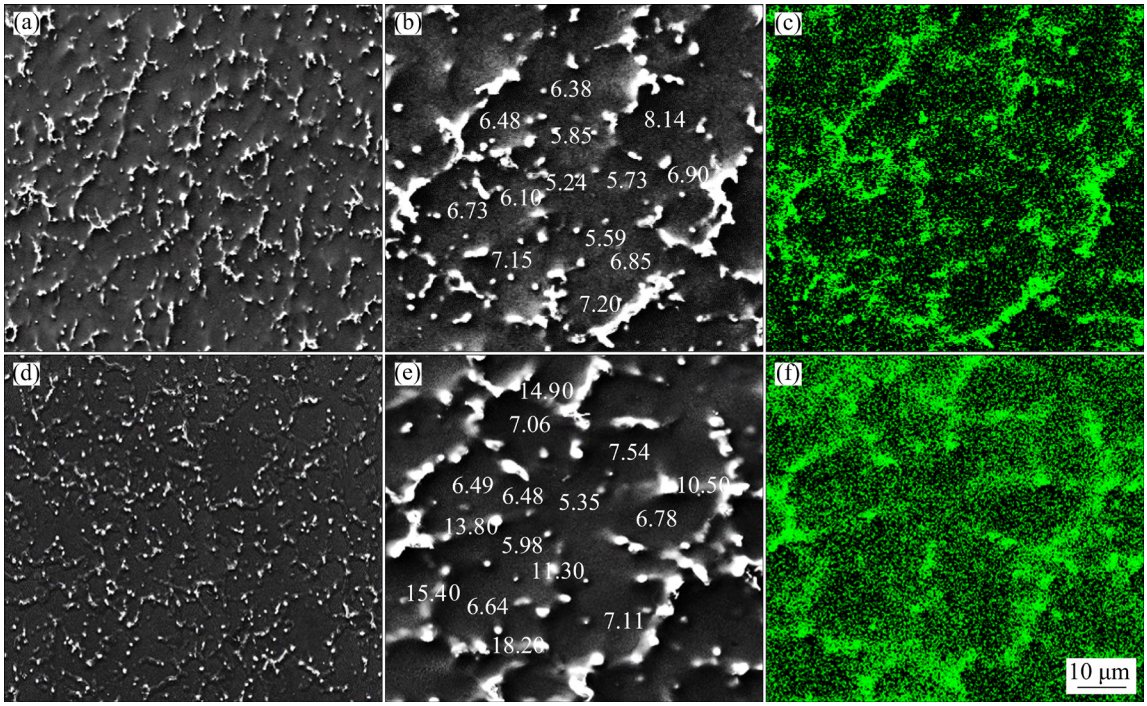

Fig. 5 Microstructure and EDS maps of Mg−11Al alloy solidified under different pressures: (a, b) Microstructure under 2 GPa; (c) EDS map under 2 GPa; (d, e) Microstructure under 3 GPa; (f) EDS map under 3 GPa

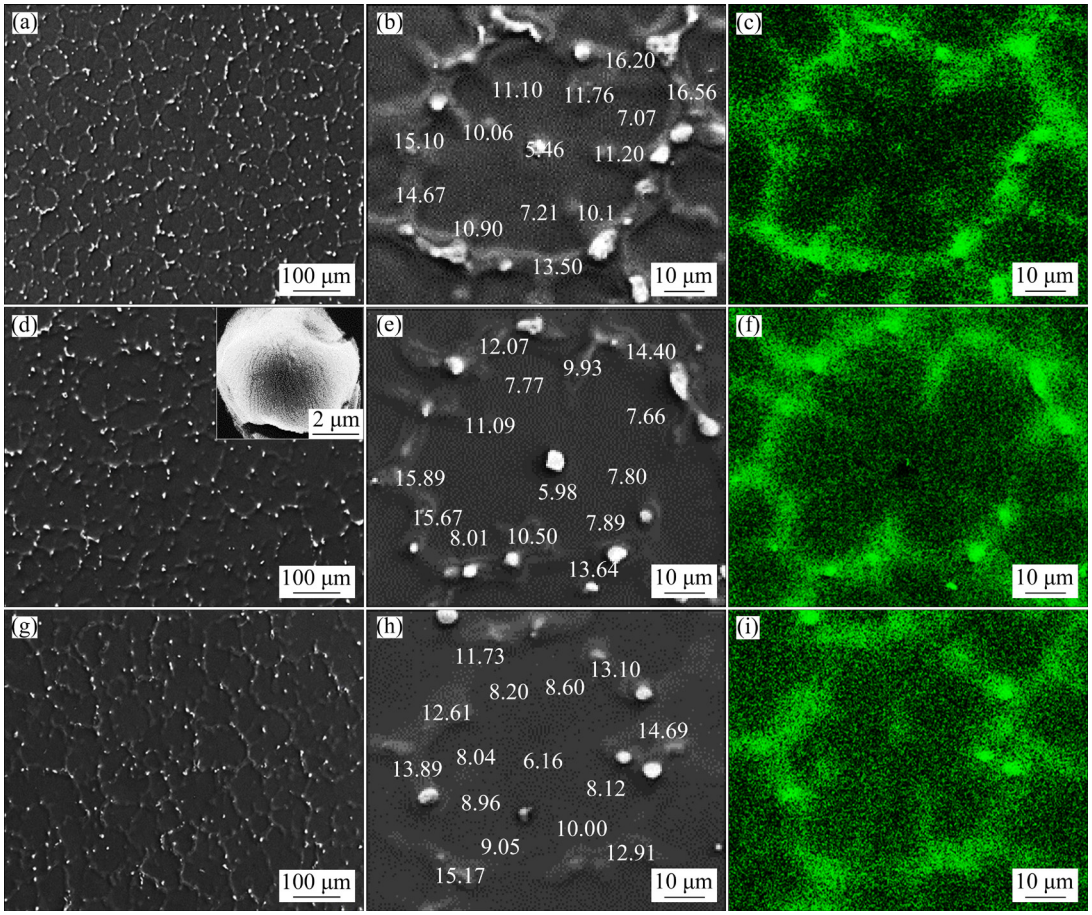

Fig. 6 Microstructure and EDS maps of typical grain planes of solidified Mg−11Al alloys under 4, 5, and 6 GPa: (a, b) Microstructure under 4 GPa; (c) EDS map under 4 GPa; (d, e) Microstructure under 5 GPa; (f) EDS map under 5 GPa; (g, h) Microstructure under 6 GPa; (i) EDS map under 6 GPa

4 GPa, the granular eutectic β-$Mg_{17}Al_{12}$ phases are mostly distributed at the triple grain boundary junctions, and the area fraction further decreases, with no eutectic phase observed inside the grains (Fig. 6(b)). Under 5 GPa, the amount of eutectic β-$Mg_{17}Al_{12}$ decreases (Fig. 6(e)), and the eutectic phase changes from a rod-like structure to a fibrous structure (the inset in Fig. 6(d)). Under 6 GPa, only a little granular eutectic β-$Mg_{17}Al_{12}$ can be seen at the α-Mg grain boundaries (Fig. 6(h)). In addition, it can be seen from Fig. 6(i) that the distribution of Al atoms in the α-Mg is more uniform under 6 GPa. Since the area fraction of the eutectic β-$Mg_{17}Al_{12}$ is less than 5% for the alloys solidified under 4−6 GPa, no diffraction peak of the β-$Mg_{17}Al_{12}$ phase is detected in the XRD pattern (Fig. 4). With increasing pressure, the quantity of the eutectic β-$Mg_{17}Al_{12}$ decreases, while more Al elements are concentrated at grain boundaries in the form of solute atoms. According to the EDS data (the numbers in Figs. 6(b, e, h)), the Al solute contents (mass fraction) at grain boundaries under 4, 5, and 6 GPa, are 13.50%−16.56%, 12.07%−15.89%, and 11.73%−15.67%, respectively. The dendrite segregation ratios under 4, 5, and 6 GPa are 1.66, 1.45, and 1.25, respectively. Accordingly, under 5 and 6 GPa, the solidification structure was significantly refined, and the degree of grain boundary (dendrite) segregation was considerably reduced. Moreover, high pressure can change the mode of occurrence of Al. Under atmospheric pressure, the element Al was distributed in eutectic β-$Mg_{17}Al_{12}$. Under high pressure, Al was distributed in the form of a solute, and the solubility of Al in the matrix increased.

3.2 Effect of solidification pressure on solute distribution in Mg−11Al alloy

Figure 7 shows the relationship between the mass fraction of the solid phase and temperature during the solidification of the Mg−11Al alloy, plotted using thermodynamic simulation software FactSage 8.0. Under equilibrium condition (Fig. 7(a)), isomorphous transformation ($L\rightarrow\alpha$-Mg) begins when the temperature drops to the liquidus temperature T_L, and the alloy enters a single α-Mg phase zone. When the temperature continues to decrease to the solubility curve, the precipitation transition occurs (α-Mg$\rightarrow\beta$-$Mg_{17}Al_{12}$). Thus, the microstructure of the alloy consists of α-Mg and

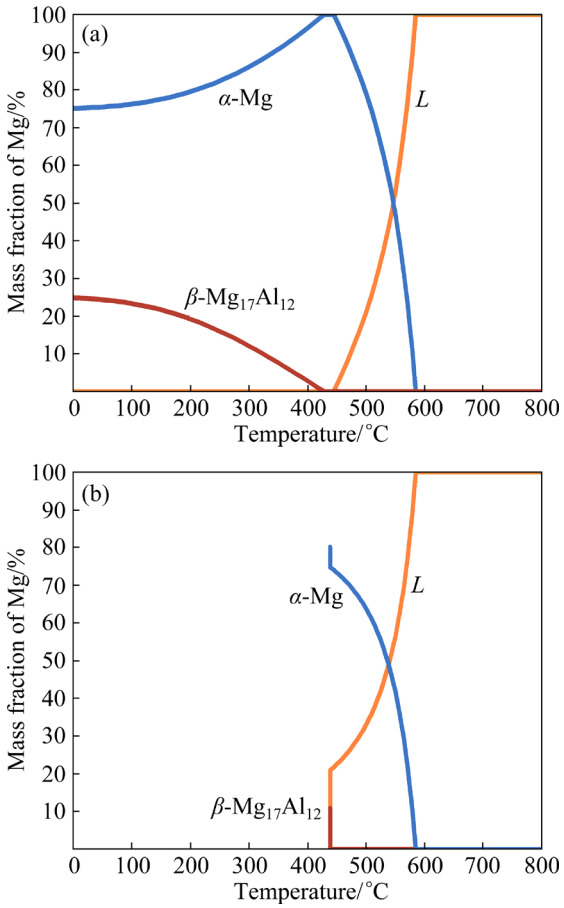

Fig. 7 Relationship between mass fraction of solid phase and temperature during solidification of Mg−11Al alloy under different conditions: (a) Equilibrium condition; (b) Scheil condition

β-$Mg_{17}Al_{12}$ at room temperature, and the mass fraction of β-$Mg_{17}Al_{12}$ is 24.81%.

Under Scheil condition (no diffusion in the solid phase, and sufficient diffusion in the liquid phase), the alloy is in a two-phase zone (L+α-Mg) after isomorphous transformation ($L\rightarrow\alpha$-Mg), as shown in Fig. 7(b). When the temperature decreases to the eutectic transformation temperature, the remaining liquid phase starts the eutectic transformation: $L\rightarrow\alpha$-Mg+β-$Mg_{17}Al_{12}$. With further decrease in temperature, precipitation transition does not occur. Therefore, the microstructure of the alloy is composed of α-Mg and α-Mg+β-$Mg_{17}Al_{12}$ eutectic at room temperature, and the mass fraction of eutectic β-$Mg_{17}Al_{12}$ is 10.84%. Thus, the microstructure is hypoeutectic under Scheil condition.

The solidification structure of the Mg−Al alloys produced by conventional casting differs from those under equilibrium and Scheil conditions.

During actual casting, the solute in the liquid phase cannot diffuse fully, similar to the Scheil condition, and only limited diffusion occurs. In reality, both diffusion and convection occur, leading to partial mixing of the solute. Without considering the diffusion of solute atoms in the solid phase, the solute concentration (C_S^*) at the solid–liquid interface under the Scheil equation can be expressed as follows [18]:

$$C_S^*=k_E C_0(1-f_S)^{k_E-1} \quad (2)$$

$$\overline{C}_L=C_0 f_L^{k_E-1} \quad (3)$$

where k_E is the effective partition coefficient, $k_E=C_S^*/C_0=k_0+(1-k_0)\exp(-R\delta_N/D_L)$, $k_0<k_E<1$, f_S and f_L are the volume fractions of the solid and liquid phases, respectively (%), R is the solidification rate (mm/s), δ_N is the thickness of the boundary layer (mm), and D_L is the diffusion coefficient of the solute element in the liquid phase (mm^2/s).

For the Mg−11Al alloy solidified under atmospheric pressure, the solidification rate was less than 10^2 K/s [19]. During solidification, the solid composition tended to homogenize because of the diffusion of Al atoms in the solid phase, and the Al content in the center of the initial solid phase (5.04 wt.%) was higher than k_0C_0 (4.07 wt.%). Therefore, C_S^* increased slightly, as shown in Fig. 8, and solute depletion in the solid phase was higher than that under Scheil condition. Simultaneously, a large amount of Al solute is pushed to the solid−liquid interface, forming a solute-rich layer (δ_N), $C_L^*<C_0/k_0$, and $C_0<\overline{C}_L<C_L^*$.

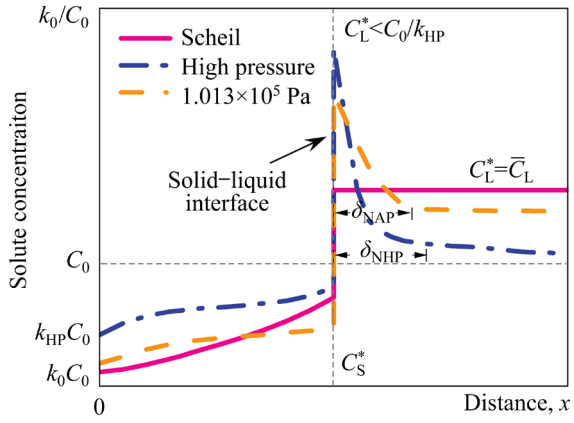

Fig. 8 Equilibrium phase diagram of binary eutectic alloys and solute redistribution under different solidification conditions (k_{HP} is solute partition coefficient under high pressures; δ_{NAP} is solute boundary layer thickness under atmospheric pressure; δ_{NHP} is solute boundary layer thickness under high pressure)

According to the mass conservation law, the total amount of excess liquid phase was higher than that under Scheil condition. Numerous studies have shown that eutectic transformation will occur when the Al content changes in the range of 4.5 wt.%−6.0 wt.% during actual casting [20]. When two growing grains meet, the excess liquid phases undergo an eutectic transformation at the grain boundaries of the solidified grains, forming a reticulate eutectic structure distributed along the grain boundaries. In addition, the lamellar β-$Mg_{17}Al_{12}$ phase will precipitate near the grain boundaries with the segregation of Al solute during the cooling process. In summary, both eutectic transformation under Scheil condition and precipitation transformation under equilibrium condition occurred during the solidification of the Mg−11Al alloy under atmospheric pressure, resulting in high grain boundary segregation and low dendrite segregation.

For the Mg−11Al alloy solidified under high pressures, the average solid solubility of Al atoms in the center of the α-Mg grains is only 6.16 wt.% even under 6 GPa, and the highest Al solubility (10.01 wt.%) among dendrites is also slightly lower than C_0 (11 wt.%). That is, $C_S^*/C_0<1$, indicating that the solute partition coefficient under high pressures k_{HP} of the Mg−Al alloy was less than 1 when the solidification pressure did not exceed 6 GPa. Under 2 GPa, there is no lamellar β-$Mg_{17}Al_{12}$ in the solidification structure of the Mg−11Al alloy (Fig. 5), showing the weak diffusion ability of Al solute in the solid phase during solidification under high pressures. Therefore, under 2−6 GPa, the solute redistribution law during the solidification of the Mg−Al alloy is more consistent with the Scheil equation.

The boundary layer thickness plays a decisive role in the solute redistribution in front of the solid−liquid interface during solidification. When C_0 is the same, the solid composition at the interface C_S^* in the stable state depends on $-R\delta_N/D_L$. With larger solidification rate R, smaller diffusion coefficient D_L, and thicker boundary layer δ_N, C_S^* is closer to C_0, then k_E is larger.

Under atmospheric pressure, the value of D_L is 5×10^{-3} mm^2/s. Under high pressures, the viscosity of the melt increases with increasing pressure [21]; thus, D_L will decrease exponentially with increasing pressure [22]. High pressure can weaken the melt

convection, leading to an increase in δ_N. In addition, the solidification rate of the alloy under high pressures (>10^2 K/s) was higher than that under atmospheric pressure [23]. Therefore, the solute partition coefficient under high pressure k_{HP} is greater than k_0 under equilibrium condition and can further increase with increasing pressure. According to the EDS data in Fig. 6, the average Al content in the center of α-Mg grains under 4, 5, and 6 GPa is 5.46 wt.%, 5.98 wt.%, and 6.16 wt.%, respectively, and the average Al content is equal to $k_{HP}C_0$ owing to no diffusion in the solid phase. Thus, the k_{HP} values of the alloys solidified under 4, 5, and 6 GPa were 0.49, 0.54, and 0.56, respectively.

Under 3−6 GPa, the initial solid composition is $k_{HP}C_0$, as shown in Fig. 8. The increase in C_S^* is higher than that under atmospheric pressure owing to the lack of diffusion in the solid phase, so solute depletion in the initial transition zone is less than that under atmospheric pressure [24]. In accordance with the law of mass conservation, the total solute depletion in the initial transition zone is equal to the total amount of excess solute in the final transition zone. Accordingly, the excess solute in the final transition zone under 3−6 GPa is less than that under atmospheric pressure.

According to the Scheil equation, the minimum Al content required is 9.82 wt.% if the Mg−Al binary alloy undergoes eutectic transformation under 4 GPa, which is higher than the Al content required under atmospheric pressure [25]. LIN et al [11] studied Mg–xAl (x=3 wt.%−40 wt.%) alloys solidified under 4 GPa and found that the microstructure is completely eutectic when the Al content was 38.28 wt.%, which means that the Al content at the eutectic point increased from 32.2 wt.% under atmospheric pressure to 38.28 wt.% under 4 GPa. Therefore, the island-like or granular eutectic phase can exist only at the triple grain boundary junctions in the final solidified area of the Mg−11Al alloy under 4 GPa. With further increase in solidification pressure, k_{HP} continues to increase, so the Al content at the eutectic point rises [26]. Under 6 GPa only a small amount of granular eutectic phase can be seen at the grain boundaries, and Al atoms are concentrated at the grain boundaries in the form of solute (content range of 12.91 wt.%−15.63 wt.%).

Under 2 and 3 GPa, the value of k_{HP} is lower than that under 4 GPa, so both the total solute depletion in the initial transition zone and the total amount of excess solute in the final transition zone are higher than those under 4 GPa. Moreover, both the minimum Al content required for eutectic transformation and the Al content at the eutectic point under 2 and 3 GPa are lower than those under 4 GPa. Therefore, the mass fraction of the eutectic phase at the grain boundaries in the final solidification area is higher than that under 4 GPa.

3.3 First-principles calculations of effect of pressure on grain boundary segregation and bonding strength of Mg−Al alloy

Figure 9 shows the doping energy and the grain boundary segregation energy of Al atoms under different pressures. The doping energy (ΔE) is calculated by [26]

$$\Delta E = E^X - E \tag{4}$$

where E^X is the total energy of twin boundaries with doped atoms, and E is the total energy of twin boundaries without doped atoms.

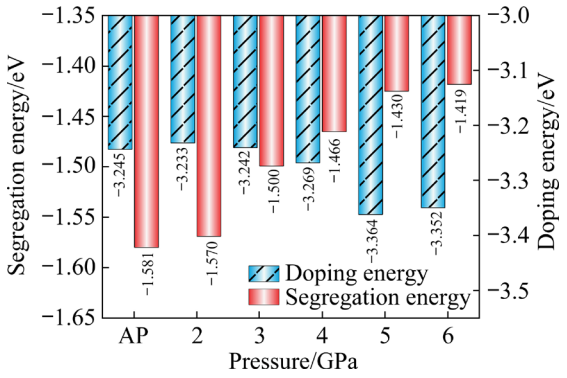

Fig. 9 Effect of pressure on grain boundary segregation energy and doping energy of Al atoms (AP represents atmospheric pressure of 1.013×10^5 Pa)

The grain boundary segregation energy (E_{seg}) is calculated by [26,27]

$$E_{seg} = (E_{GB}^X - E_{SR}) - (E_{Bulk}^X - E_{Bulk} - E_{Al}) \tag{5}$$

where E_{GB}^X is the total energy of the system when Al atoms at the grain boundaries are at compression or expansion sites, E_{Bulk}^X is the total energy of the system when Al atoms are doped in Mg unit cells, E_{SR} is the total energy of the system when Al atoms at the grain boundaries are at the doping sites (the small dashed rectangle in Fig. 2), E_{Bulk} is the total energy of the Mg unit cells, and E_{Al} is the total energy of Al atoms.

The doping energy of Al atoms is −3.245 eV under atmospheric pressure, −3.233 eV under 2 GPa, and −3.242 eV under 3 GPa, as shown in Fig. 9. When the pressure reaches 4 GPa, the doping energy of Al atoms is lower than that under atmospheric pressure. Afterward, the doping energy gradually decreases from −3.269 eV under 4 GPa to −3.352 eV under 6 GPa, indicating that the stability of the Mg−Al alloy is higher under 4−6 GPa.

Under atmospheric pressure, the grain boundary segregation energy of Al atoms is −1.581 eV. Under 2 GPa, the grain boundary segregation energy is −1.570 eV, which is slightly higher than that under atmospheric pressure. When the pressure exceeds 3 GPa, the grain boundary segregation energy of Al atoms rises with increasing pressure, from −1.500 eV under 3 GPa to −1.466 eV under 4 GPa and −1.419 eV under 6 GPa, indicating that under 4−6 GPa, the grain boundary segregation of Al atoms can be significantly reduced.

During solidification under 4−6 GPa, the doping energy of Al atoms is lower than that under atmospheric pressure, but the grain boundary segregation energy is higher than that under atmospheric pressure, so the solidification pressure affects the distribution of Al atoms. Figure 10 shows the effect of pressure on the solubility energy of Al atoms in α-Mg and the binding energy of β-$Mg_{17}Al_{12}$. The solubility energy of Al atoms in α-Mg (E_{sol}^{Al-Mg}) can be calculated by [27]

$$E_{sol}^{Al-Mg} = E_{Bulk}^{119Mg-1Al} - E_{Bulk}^{119Mg} - E_{Al} \quad (6)$$

where $E_{Bulk}^{119Mg-1Al}$ is the total energy of the Mg matrix containing 119 Mg atoms and 1 Al atom, E_{Bulk}^{119Mg} is the total energy of 119 Mg atoms, and E_{Al} is the energy of 1 Al atom.

Binding energy of β-$Mg_{17}Al_{12}$ ($E_{col}^{\beta\text{-}Mg_{17}Al_{12}}$) can be calculated by [28]

$$E_{col}^{\beta\text{-}Mg_{17}Al_{12}} = E_{\beta\text{-}Mg_{17}Al_{12}} - 17E_{Mg} - 12E_{Al} \quad (7)$$

where $E_{\beta\text{-}Mg_{17}Al_{12}}$ represents the total energy of β-$Mg_{17}Al_{12}$, and E_{Mg} is the energy of 1 Mg atom.

As shown in Fig. 10(a), the solubility energy of Al atoms in α-Mg is 1.293 eV under atmospheric pressure, and 1.300 eV under 2 GPa. Afterwards, the solubility energy decreases with increasing pressure, from 1.243 eV under 3 GPa to 1.138 eV under 6 GPa. Consequently, the stability of Al atoms dissolved in α-Mg is enhanced with increasing pressure from 3 to 6 GPa.

As shown in Fig. 10(b), the binding energy of β-$Mg_{17}Al_{12}$ is −1.660, −1.663, and −1.720 eV under atmospheric pressure, 2 GPa, and 6 GPa, respectively. Thus, the binding energy gradually decreases with increasing pressure. Therefore, the stability of the $Mg_{17}Al_{12}$ phase increases with increasing pressure.

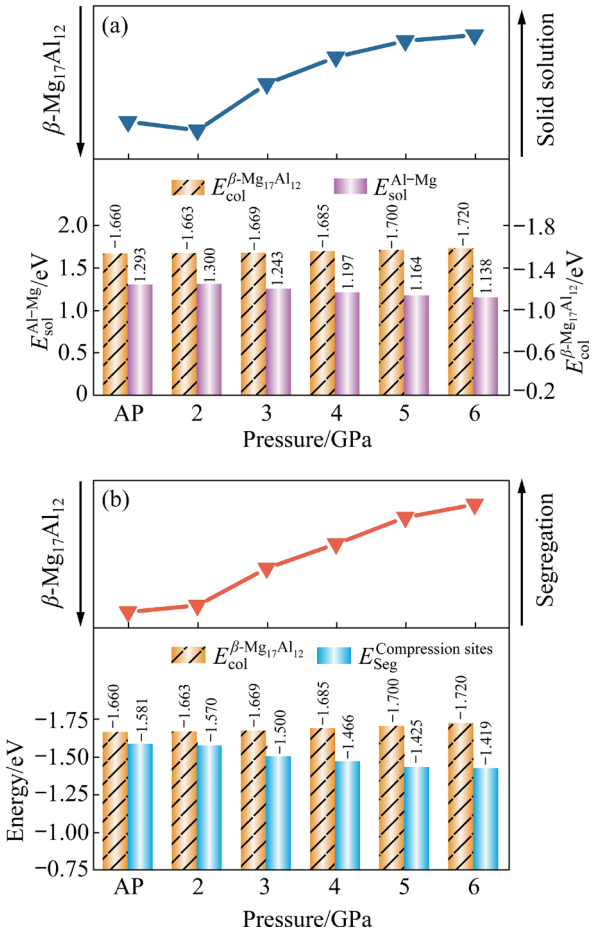

Fig. 10 Effect of pressure on solid solution (a) and segregation (b) of Al atoms

According to the red curve in Fig. 10(b), Al atoms tend to distribute at the grain boundaries in the form of solute atoms with increasing pressure, so high pressure can suppress the formation of the β-$Mg_{17}Al_{12}$ phase. According to the blue curve in Fig. 10(a), more Al atoms tend to dissolve in α-Mg under 3−6 GPa. These conclusions can be confirmed by the eutectic phase morphology and the EDS data in Figs. 5 and 6.

Figure 11 shows the differential charge density of grain boundary segregation in different pressure ranges, where the red area represents electron enrichment and the blue area represents electron

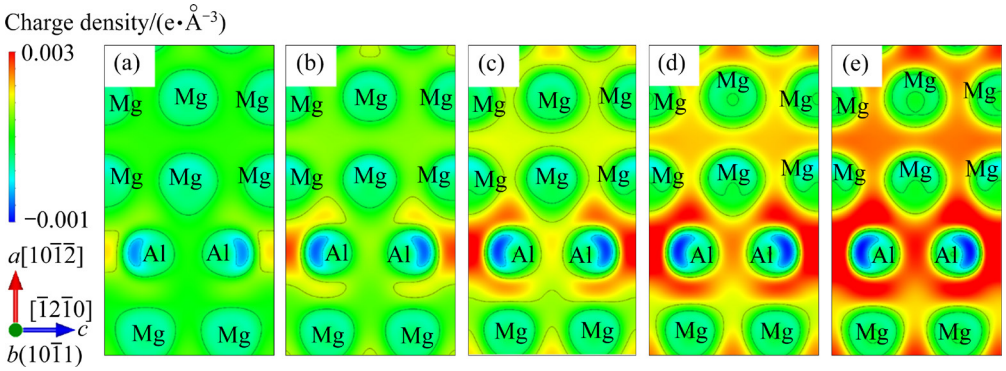

Fig. 11 Effect of pressure range on differential charge density of grain boundary segregation of Al atoms: (a) AP−2 GPa; (b) AP−3 GPa; (c) AP−4 GPa; (d) AP−5 GPa; (e) AP−6 GPa

depletion. In the pressure range of AP−2GPa, the charge density between Mg and Al atoms increases slightly, while the charge density between Al and Al, and Mg and Mg atoms hardly changes. In the pressure range of AP−3 GPa, the charge density between Mg and Al atoms further increases, and the charge density between Al and Al, and Mg and Mg atoms also rises. In the pressure ranges of AP−4 and AP−5 GPa, the charge density between Mg and Al, Al and Al, and Mg and Mg atoms increases with increasing pressure, and the charge density between Al and Al atoms increases faster than that between Mg and Mg atoms. In the pressure range of AP−6 GPa, the charge density between Mg and Al, Al and Al, and Mg and Mg atoms is significantly enhanced. Thus, the strength of Mg—Al, Al—Al, and Mg—Mg bonds is improved when the pressure exceeds 3 GPa, especially under AP−6 GPa. In summary, under high pressure of GPa-level, the grain boundary segregation of Al solute increases the bond strength of grain boundaries and inhibits grain boundary sliding.

4 Conclusions

(1) The microstructure of the Mg−11Al alloys solidified under 2−6 GPa consists of α-Mg and β-$Mg_{17}Al_{12}$ along grain boundaries, without lamellar β-phase. Under 2 GPa, severe dendrite segregation can be seen. Under 3−6 GPa, the grains are refined and more equiaxed.

(2) The morphology of the eutectic β-$Mg_{17}Al_{12}$ changes from an island-like distribution under 3 GPa to a granular distribution under 5−6 GPa, and the area fraction of the eutectic β-$Mg_{17}Al_{12}$ decreases from 8.1% under 3 GPa to less than 2% under 5−6 GPa. In addition, the Al content in the center of α-Mg grains increases, and the Al content among dendrites decreases, with more Al solutes at the grain boundaries, as the pressure increases from 3 to 6 GPa.

(3) The solute partition coefficient under high pressures k_{HP} of the Mg−11Al alloy is less than 1 and increases with increasing pressure. The solute redistribution law during solidification is consistent with the Scheil equation. Under 4−6 GPa, the eutectic transformation is gradually suppressed owing to the high k_{HP} and large undercooling.

(4) With increasing pressure, the grain boundary doping energy of the Al atoms decreases, and the grain boundary segregation energy of the Al atoms increases. The grain boundary segregation of Al atoms during solidification under high pressures can increase the bond strength of the grain boundaries and restrain grain boundary sliding during loading.

CRediT authorship contribution statement

Shi-min AI: Validation, Formal analysis, Writing – Original draft; **Xiao-ping LIN:** Conceptualization, Writing – Review & editing; **Yao-wei GUO:** Methodology, Data curation; **Xu-zhao ZHANG:** Visualization; **Da-ran FANG:** Project administration, Writing – Review & editing; **Lian-wei YANG:** Supervision; **Bin WEN:** Calculation guidance.

Declaration of competing interest

The authors declare that they have no known competing financial interests or personal relationships that could have appeared to influence the work reported in this paper.

Acknowledgments

This research was financially supported by the National Natural Science Foundation of China (No. 51675092), and the Natural Science Foundation of Hebei Province, China (Nos. E2022501001, E2022501006).

References

[1] TOLOUIE E, JAMAATI R. Effect of β-$Mg_{17}Al_{12}$ phase on microstructure, texture and mechanical properties of AZ91 alloy processed by asymmetric hot rolling [J]. Materials Science and Engineering: A, 2018, 738: 81−89.

[2] WEILER J P. Exploring the concept of castability in magnesium die-casting alloys [J]. Journal of Magnesium and Alloys, 2021, 9(1): 102−111.

[3] CAI Hui-sheng, WANG Zhen-zhu, LIU Liang, LI Yu-guang, GUO Feng. Regulation mechanism of cooling rate and RE (Ce, Y, Gd) on $Mg_{17}Al_{12}$ in AZ91 alloy and its role in fracture process [J]. Journal of Materials Research and Technology, 2022, 19: 3930−3941.

[4] ZUBAIR M, FELTEN M, HALLSTEDT B, PAREDES M V, ABDELLAOUI L, BILLORO P B, LIPINSKA-CHWALEK ML, AYEB N, SPRINGER H, MAYER J, BERKEL B, ZANDER D, KORTE-KERZEL S, SCHEU C, ZHANG S Y. Laves phases in Mg−Al−Ca alloys and their effect on mechanical properties [J]. Materials & Design, 2023, 225: 111470.

[5] CHE Hong-mei, JIANG Xian-quan, QIAO Nan, LIU Ziao-kui. Effects of Er/Sr/Cu additions on the microstructure and mechanical properties of Al−Mg alloy during hot extrusion [J]. Journal of Alloys and Compounds, 2017, 708: 662−670.

[6] LIU Wen-jun, JIANG Bin, YANG Qing-shan, TAO Jian-quan, LIU Bo, PAN Fu-sheng. Effect of Ce addition on hot tearing behavior of AZ91 alloy [J]. Progress in Natural Science: Materials International, 2019, 29(4): 453−456.

[7] KIRKWOOD D H. Microsegregation [J]. Materials Science and Engineering, 1984, 65(1): 101−109.

[8] RAPPAZ M, THÉVOZ P H. Solute diffusion model for equiaxed dendritic growth [J]. Acta Metallurgica, 1987, 35(7): 1487−1497.

[9] SOBCZAK J J, DRENCHEV L, ASTHANA R. Effect of pressure on solidification of metallic materials [J]. International Journal of Cast Metals Research, 2012, 25(1): 1−14.

[10] JIE J C, ZOU C M, WANG H W, LI B, WEI Z J. Enhancement of mechanical properties of Al−Mg alloy with a high Mg content solidified under high pressures [J]. Scripta Materialia, 2011, 64(6): 588−591.

[11] LIN Xiao-ping, DAI Peng-lin, XU Chang, FANG Da-rang, GUO Kun-yu, REN Zheng. Solute redistribution and mechanism of structure refinement of Mg−Al alloy during solidification under high pressure [J]. Journal of Alloys and Compounds, 2022, 910: 164777.

[12] XU Chang, ZHANG Zhu-qun, DAI Peng-lin, KUO Yang, LIN Xiao-ping. Preparation of fibrous γ-$Mg_{17}Al_{12}$ eutectic phase and its effect on mechanical properties of Mg alloy [J]. Foundry, 2021, 70(8): 915−920. (Chinese)

[13] LIN Xiao-ping, KUO Yang, WANG Lin, YE Jie, ZHANG Chong, WANG Li, GUO Kun-yu. Refinement and strengthening mechanism of Mg−Zn−Cu−Zr−Ca alloy solidified under extremely high pressure [J]. Transactions of Nonferrous Metals Society of China, 2021, 31(6): 1587−1598.

[14] GUO Kun-yu, XU Chang, LIN Xiao-ping, YE Jie, ZHANG Chong, HUANG Duo. Microstructure and strengthening mechanism of Mg−5.88Zn−0.53Cu−0.16Zr alloy solidified under high pressure [J]. Transactions of Nonferrous Metals Society of China, 2020, 30(1): 99−109.

[15] HONG Q J, AXEL V. Reentrant melting of sodium, magnesium, and aluminum: General trend [J]. Physical Review B, 2019, 100: 140102.

[16] KRESSE G, FURTHMÜLLER J. Efficiency of ab-initio total energy calculations for metals and semiconductors using a plane-wave basis set [J]. Computational Materials Science, 1996, 6(1): 15−50.

[17] ADAMO C, BARONE V. Toward reliable density functional methods without adjustable parameters: The PBE0 model [J]. The Journal of Chemical Physics, 1999, 110(13): 6158−6170.

[18] WANG Lin, LIN Xiao-ping, XU Chang, ZHAO Sheng-shi, SUN Heng, ZHANG Ning. The microstructure and the mechanical property of AZ91D solidified under GPa-grade high-pressure [J]. Materials Science and Technology, 2019, 35(6): 1690−1699.

[19] BERMAN T D, YAO Zhen-jie, DEDA E, GODLEWSKI L, LI Mei, ALLISON J E. Measuring and modeling micro-segregation in high-pressure die cast Mg−Al alloys [J]. Metallurgical and Materials Transactions A, 2022, 53(7): 2730−2742.

[20] FATMI M, DJEMLI A, OUALI A, CHIHI T, GHEBOULI M A, BELHOUCHET H. Heat treatment and kinetics of precipitation of β-$Mg_{17}Al_{12}$ phase in AZ91 alloy [J]. Results in Physics, 2018, 10: 693−698.

[21] HUANG Xiao-ran, HAN Zhi-qiang, LIU Bai-cheng. Study on the effect of pressure on the equilibrium and stability of the solid−liquid interface in solidification of binary alloys [J]. Science China Technological Sciences, 2011, 54, 479−483.

[22] WANG Hong-wei, ZHU Dong-dong, ZOU Chun-ming, WEI Zun-jie. Evolution of the microstructure and nanohardness of Ti−48at.%Al alloy solidified under high pressure [J]. Materials & Design, 2012, 34: 488−493.

[23] SHARIFI P, JAMALI J, SADAYAPPAN K, WOOD J T. Grain size distribution and interfacial heat transfer coefficient during solidification of magnesium alloys using high pressure die casting process [J]. Journal of Materials Science & Technology, 2018, 34(2): 324−334.

[24] RONG Jian, XIAO Wen-long, FU Yu, ZHAO Xin-qing, YAN Peng, MA Chao-li, CHEN Ming, HUANG Chen. A high performance Mg−Al−Ca alloy processed by high pressure die casting: Microstructure, mechanical properties and thermal conductivity [J]. Materials Science and Engineering: A, 2022, 849: 143500.

[25] ZUO Y, CHANG Y A. Thermodynamic calculation of the Al−Mg phase diagram [J]. Calphad, 1993, 17(2): 161−174.

[26] LIN Xiao-ping, DANG Yu-zhen, DAI Peng-lin, FANG

Da-rang, XU Chang, WEN Bin. Microstructure control and strengthening mechanism of fine-grained cast Mg alloys based on grain boundary segregation of Al solute [J]. Materials Science and Engineering: A, 2022, 851: 143665.

[27] HUI Jun, ZHANG Xiao-yong, LIU Tao, LIU Wen-guan, WANG Biao. First-principles calculation of twin boundary energy and strength/embrittlement in hexagonal close-packed titanium [J]. Materials & Design, 2022, 213: 110331.

[28] PEI Zong-rui, LI Rui, NIE Jian-feng, MORRIS J R. First-principles study of the solute segregation in twin boundaries in Mg and possible descriptors for mechanical properties [J]. Materials & Design, 2019, 165: 107574.

高压对 Mg−11Al 合金显微组织和微观偏析的影响

艾士民[1]，林小娉[1,2]，郭耀威[1]，张旭婴[1]，房大然[1,2]，杨连威[1,2]，温 斌[3]

1. 东北大学 材料科学与工程学院，沈阳 110819；
2. 东北大学秦皇岛分校 资源与材料学院，秦皇岛 066004；
3. 燕山大学 材料科学与工程学院，秦皇岛 066004

摘 要：基于实验与第一性原理计算相结合研究了高压对 Mg−11Al(质量分数，%)合金显微组织和微观偏析的影响。结果表明，在 4~6 GPa 高压下凝固的 Mg−11Al 合金具有较大的溶质分配系数及过冷度，使先结晶的固相中 Al 含量较高、且 Al 含量随压力升高而增加，因此，最终凝固阶段液相中过剩溶质总量随压力增加而减少，从而减少或抑制共晶转变。当压力为 5~6 GPa 凝固时，合金显微组织为由具有较高 Al 原子溶解性的晶粒和含有大量 Al 溶质的晶界组成的细晶固溶体。随压力的升高，Al 原子晶界掺杂能降低，晶界偏析能增加，Mg—Al (Mg)健间电荷密度增大，因此提高了显微组织的稳定性和晶界的键合强度。

关键词：高压凝固；晶界偏析；分配系数；Mg−Al 合金；固溶体

(Edited by Wei-ping CHEN)